

2C. The image shows columns with a well-defined spacing and a single orientation. This is verified by the FT of the image (Fig. 2D), in which only a single reflection (and its inverse) are evident, corresponding to the repeat units for the columnar separation.

Another feature of our AFM images (see Fig. 2C) is the appearance of maxima along the tops of the columns, which have a characteristic spacing but which are not correlated in position from column to column. This feature is not manifested in the FT images for two reasons. First, the short range of the intracolumnar order should convert sharp peaks in the FT into radial streaks. Second, the lack of intercolumnar correlations (that is, the lack of column-to-column registry of the disks) should further broaden these streaks into weak diffuse maxima. Both types of broadening have been seen in XRD studies of oriented strands of discotic liquid crystals (18); the sharp peak corresponding to the intercolumnar spacing is typically two to three orders of magnitude more intense than the diffuse peak corresponding to short-range intracolumnar order. In principle, therefore, the intracolumnar order would be visible as a diffuse feature in the FT of an AFM image with several more decades of dynamic range.

The details of the intracolumnar structure can be seen more clearly in Fig. 2E, which shows the surface profile for a cross section along the top of the column located in the center of the AFM image from Fig. 2C. A statistical analysis of the peak separations (21) along all the columns in Fig. 2C shows an average separation of 5.14 Å with a standard deviation of 1.29 Å. If, as suggested earlier, the flexible hydrocarbon tails point up and away from the interface, the AFM tip would tend to interact with them during scanning. However, even with some spread of orientations of the tails, which may be due both to the tip interactions and to the thermally induced motions of the tails, the AFM images show that intracolumnar spacing of the disks ranges from 3.85 to 6.43 Å, in good qualitative agreement with the results of bulk XRD studies presented above.

The observed orientational ordering of this system containing strongly interacting π -conjugated systems suggests its potential for electronic and optical device applications. The clarity that AFM brings to the characterization of these LB films will be valuable in efforts to produce the defect-free, highly oriented films that are essential for such applications.

REFERENCES AND NOTES

1. S. Jin, T. H. Tiefel, R. Wolfe, R. C. Sherwood, J. J. Mottine, Jr., *Science* **255**, 446 (1992).
2. A. Ulman, *Introduction to Ultrathin Organic Films* (Academic Press, Boston, 1991).

3. S. Chandrasekhar and G. S. Ranganath, *Rep. Prog. Phys.* **53**, 57 (1990).
4. D. W. Kalina and S. W. Crane, *Thin Solid Films* **134**, 109 (1985).
5. C. Mertesdorf and H. Ringsdorf, *Liq. Cryst.* **5**, 1757 (1989).
6. N. C. Maliszewskij *et al.*, *J. Phys. II (France)* **2**, 75 (1992).
7. O. Albrecht *et al.*, *Colloid Polym. Sci.* **264**, 659 (1986).
8. O. Karthaus *et al.*, *Langmuir* **8**, 2279 (1992).
9. L. Y. Chiang *et al.*, *Mol. Cryst. Liq. Cryst.* **125**, 279 (1985); G. B. M. Vaughan *et al.*, *Phys. Rev. B* **46**, 2787 (1992).
10. E. Orthmann and G. Wegner, *Angew. Chem.* **98**, 1114 (1986).
11. D. P. E. Smith *et al.*, *Proc. Natl. Acad. Sci. U.S.A.* **84**, 969 (1987); J. P. Rabe and S. Buchholz, *Phys. Rev. Lett.* **66**, 2096 (1991).
12. G. Binnig *et al.*, *Phys. Rev. Lett.* **56**, 930 (1986).
13. G. Binnig *et al.*, *Europhys. Lett.* **3**, 1281 (1987); T. R. Albrecht and C. F. Quate, *J. Vac. Sci. Technol. A* **6**, 271 (1988).
14. T. R. Albrecht and C. F. Quate, *J. Appl. Phys.* **62**, 2599 (1987); S. Alexander *et al.*, *ibid.* **65**, 164 (1989).
15. T. R. Albrecht *et al.*, *ibid.* **64**, 1178 (1988).
16. H. G. Hansma *et al.*, *Langmuir* **7**, 1051 (1991); E. Meyer *et al.*, *Nature* **349**, 398 (1991); D. K. Schwartz, G. Garnaes, R. Viswanathan, J. A. N. Zasadzinski, *Science* **257**, 508 (1992); C. J. Eckhardt *et al.*, *Langmuir* **8**, 2591 (1992).
17. G. Wenz, *Makromol. Chem. Rapid Commun.* **6**, 577 (1985).
18. E. Fontes *et al.*, *Phys. Rev. A* **37**, 1329 (1988).
19. J. Sagiv, *J. Am. Chem. Soc.* **102**, 92 (1980).
20. Obtained from Digital Instruments, Santa Barbara, CA.
21. For this analysis, any maximum in the linear trace of a surface profile was taken to be a peak. The average separations and standard deviation were quite insensitive to the method of peak identification.
22. We thank G. Farrington, R. Reynolds, and A. Chester for support. We also thank J. K. Blasie for the use of his Langmuir trough. Financial support was provided by National Science Foundation grants DMR MRL 92-20668 and DMR 89-01219.

14 October 1992; accepted 13 January 1993

The Drift of Saturn's North Polar Spot Observed by the Hubble Space Telescope

John Caldwell, Xin-Min Hua, Benoit Turgeon,
James A. Westphal, Christopher D. Barnet

Polar projections of 50 images of Saturn at 889 nanometers and 25 images at 718 nanometers taken by the Hubble Space Telescope in November 1990, as well as 3 images at each wavelength taken in June 1991, have been examined. Among them, 31 show the north polar spot, which is associated with Saturn's polar hexagon, in locations suitable for measurement. In each image, planetocentric coordinates of the polar spot were determined, and the movement of the spot with respect to Saturn's system III rotation rate was studied. During the period of observation, the polar spot had first a short-term westward movement and then a long-term eastward drift. The rate of the long-term drift was -0.060 ± 0.008 degrees per day with respect to system III, approximately 50 percent greater than previously determined from Voyager. The original 1980 and 1981 Voyager data were combined with the new Hubble images to form an 11-year base line. The eastward drift over the longer period was -0.0569 degrees per day. The long-term drift could be due to uncertainty in the standard value of the internal rotation period, which is 810.7939 ± 0.148 degrees per 24-hour day. The short-term movement in November 1990 has a rate that is greater in magnitude but opposite in sign and probably represents a real, transient motion of the spot relative to the internal rotation system.

The hexagonal feature around Saturn's north pole was discovered by Godfrey (1) using Voyager 1 and 2 images. To investigate its dynamic characteristics, Godfrey (2) measured the rotation rate of a large spot associated with the hexagon in polar projections of the images. In his study and this study, the longitude system is defined by the system III rotation rate (3), which is

the rotation rate of the magnetic field and is believed to be related to the internal rotation. From seven images that spanned a period of ~ 270 days, he obtained a drift rate of the spot relative to the internal period, $(-8.13 \pm 0.6) \times 10^{-9}$ rad s^{-1} . It was not clear at the time whether the rate difference represented a real drift of the spot or inaccuracy in the standard value of the internal rotation rate. The existence of the hexagonal feature and the associated polar spot in 50 Hubble Space Telescope (HST) near-infrared images a decade later shows that these features are a persistent phenomenon on Saturn. The larger HST database enables us to make more precise measurements of the movement of these features.

We examined 31 images of Saturn, span-

J. Caldwell and B. Turgeon, Space Astrophysics Laboratory, Institute for Space and Terrestrial Science, and Department of Physics and Astronomy, York University, North York, Ontario, Canada M3J 1P3.
X.-M. Hua and C. D. Barnet, Space Astrophysics Laboratory, Institute for Space and Terrestrial Science, North York, Ontario, Canada M3J 3K1.
J. A. Westphal, Division of Geological and Planetary Sciences, California Institute of Technology, Pasadena, CA 91125.

ning a period of 210 days (4, 5), in which the polar spot was in a position favorable for measurement. The images were taken with the HST Planetary Camera (PC) with the use of filters centered at wavelengths of 889 and 718 nm. We found, in addition to a long-term change in the position of the spot relative to the system III, in agreement with Godfrey (2), a more rapid, short-term movement in the opposite direction during the first few days of observation. Whereas the former could be attributed to the uncertainty in the radio period, as Godfrey (2) originally suggested, the latter represents a real, transient drift of the spot relative to the internal rotation system.

The raw images taken by the HST PC contain band columns, bad rows, dust rings, and blemishes. These were removed by various methods (4-6) that do not affect the scientific conclusions herein. We then used a deconvolution algorithm developed by Cunningham and Anthony (7) which was adapted from Lucy (8).

The first step toward the determination of the location of a feature on a planet's surface is to locate the center of the planet. The rings of Saturn were used to determine the planet center because the rings have a much more clear-cut edge than the planet itself. Those results have been corroborated independently by a second analysis based on simultaneous ring and planetary limb fitting. We were seeking the center of the ellipse defined by the edge of Saturn's rings. A multiple regression method was used to find the ellipse that best fit the measured ring-edge points. This ellipse was specified by its major axis R , the orientation of its minor axis, and the center coordinates (x_0, y_0) in xy plane. The major axis, which is also the radius of the outer edge of the outer ring, and the center coordinates are given in terms of pixels, and the orientation of the minor axis is given by its angle with respect to the x -axis. We scanned each image along 40 lines, sampling about 80 points, so the uncertainty is <0.5 pixel.

To transform the image coordinates into the planet's proper coordinate system, we approximated the planet as an oblate spheroid, its equatorial and polar radius being a and b , respectively. For Saturn, $a = 60,268$ km, $a/R = 0.43857$, and $b/a = 0.8924$. We used polar orthographic projection (9) for the precise measurement of the movement of the near-polar spot. The coordinates of the center of the polar spot in the projected images were found with the use of a method that computes the centroid of the spot region with the criterion that local derivatives of the brightness are zero at the centroid. The location is then converted to longitude and latitude (9). The longitude so determined is relative to Saturn's central meridian and can be easily converted to system III longitude.

Accurate determination of longitudes and latitudes of the spot on Saturn's surface depends on correct polar projection. The polar projection, in turn, depends critically on the planetary radius. At first, we used the values obtained by multiplying R from our ring-edge fitting by the ratio of a/R , which gave an equatorial radius in pixels. The conversion factor between the dimension of the planet in pixel and the angular size, as determined from the *Astronomical Almanac*, is invariably 0.0441 arc sec/pixel.

Using these values of radius, we did initial polar projections and spot location measurements. We found a correlation between the angular distance of the spot from the central meridian and the measured longitude and latitude. However, there is no plausible physical reason for such a correlation. We believe that this is a systematic error caused by an incorrect scale factor in our initial analysis. The measured scale of 0.0441 arc sec/pixel, which is significantly larger than the value of 0.043 arc sec/pixel expected with HST optics, cannot be explained by image-smearing effects because these should decrease the measured scale

(for example, the rings would appear larger than they really are).

To confirm the systematic error in the initial analysis, we calculated a series of apparent longitudes and latitudes for various locations of a trial point relative to the central meridian, allowing the image to have a slightly different scale factor. The calculations verified the behavior of both the longitude and latitude values that we observed and revealed that the original image scale

Table 1. Position of the polar spot. Longitude has been converted to system III and latitude is measured from the equator. Time is in minutes from 00:00:00 universal time (UT) on 9 November 1990.

Time (min)	Longitude (degrees west)	Latitude (degrees north)
<i>889-nm images</i>		
467	123.6	72.0
469	123.2	71.9
471	122.4	71.7
473	121.0	72.0
564	124.8	72.1
566	123.1	72.1
568	124.9	72.0
570	124.2	71.8
3,684	126.5	71.8
3,686	125.7	71.8
3,688	127.6	71.9
3,690	126.1	71.9
12,002	128.1	72.0
12,082	132.5	71.6
12,084	131.6	71.8
12,086	133.2	71.7
13,246	133.0	72.3
13,248	130.9	72.3
13,244	132.2	72.5
13,356	131.2	72.2
13,358	131.3	72.1
13,438	130.9	72.3
13,440	132.1	71.8
13,442	131.7	71.8
301,040	115.1	72.7
<i>718-nm images</i>		
12,005	128.0	71.8
12,109	125.8	72.0
12,111	135.7	71.2
13,271	133.5	71.6
13,361	138.3	71.7
301,046	115.2	72.9

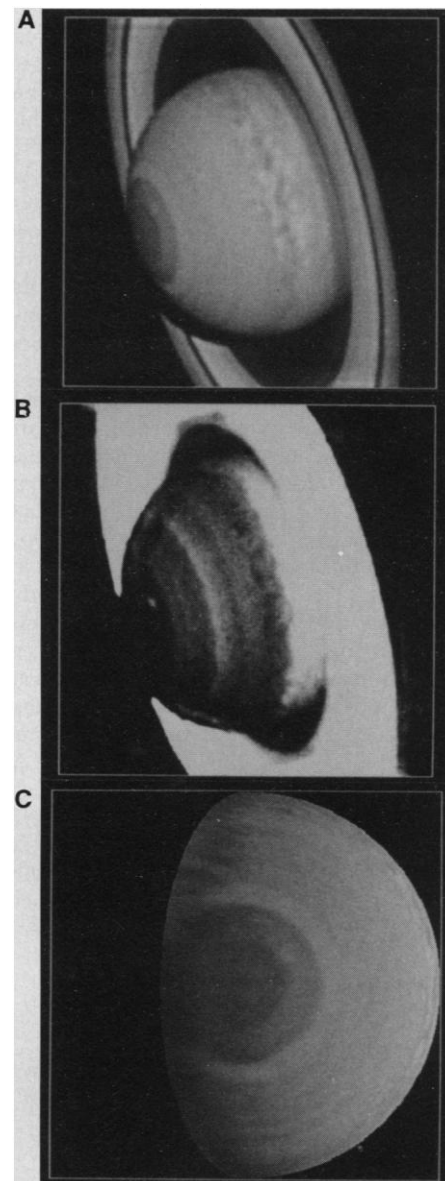


Fig. 1. Images of Saturn and its ring at (A) 718 nm and (B) 889 nm. The image in (B) has been contrast enhanced, which saturates the ring but allows one to view the planetary features. This image does not deconvolve well because of the large contrast differences between the ring and planet. This problem does not affect the position of the polar spot. Some evidence of the Saturnian equatorial storm from September 1990 is still visible in this November image. (C) The polar-projected view of the image in (A).

was incorrect by a factor of 1.014. This change in radius is equivalent to a change in pixel size to 0.0435 arc sec/pixel, which is in fair agreement with the standard value of 0.043 arc sec/pixel, and may be considered an improvement. In essence, the rings were used to determine the planet center, and the wandering of the polar spot on a time scale of hours was minimized to determine the image scale. This implies that the HST PC has a geometric distortion that is larger at the edges of the charge-coupled device (CCD) detector.

The 50 images of Saturn taken through the 889-nm filter and the 25 images taken through the 718-nm filter in November 1990 by the HST PC were used for the polar spot investigation. Six additional images taken through both filters in June 1991 greatly extended the temporal base line. At 889 nm, only 24 images from the November 1990 sequence and 1 in June 1991 show the polar spot in a location favorable for measurement. For the 718-nm images, only five from the November 1990 set and one from the June 1991 set have the polar spot favorably placed.

For each image, we determined the center of the planet by ring-edge fitting, polar-projected the image, and determined the latitude and longitude of the polar spot (Table 1). Both the spot and hexagonal features can be seen at 718 nm (Fig. 1A), although the spot contrast is quite low. On the other hand, only the spot is clearly visible at 889 nm (Fig. 1B), but at this wavelength, the contrast is very high. The 889-nm image was useful for confirmation of the spot's location. The white spot near one facet of the hexagon can be seen in the polar projection of the image in Fig. 1A (Fig. 1C).

At both wavelengths, the spot has a movement relative to system III. In Fig. 2, the positions of the polar spot for both wavelengths are shown. The time sequence is illustrated by lines connecting the mea-

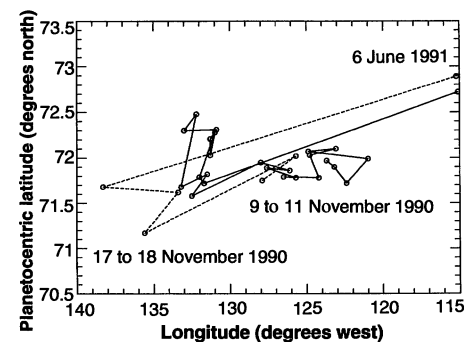


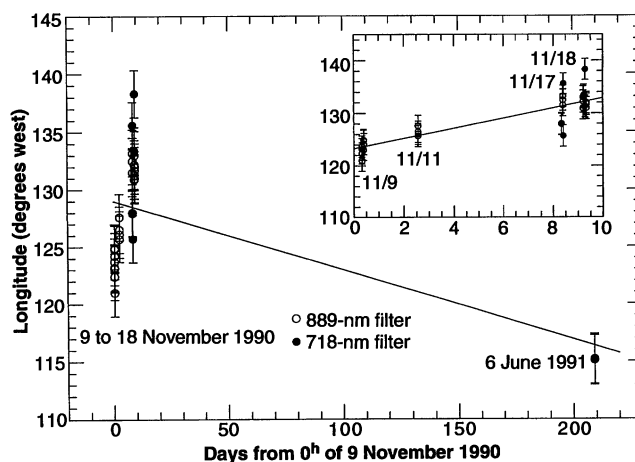
Fig. 2. Movement of the polar spot. Circles are measurements from Table 1. Lines track values for the 889-nm filter (solid line) and 718-nm filter (dashed line).

surements. The movement was westward during the 9-day period in November 1990 but eastward over the 209-day period from November 1990 to June 1991.

In Fig. 3, we plot the longitude variation with time for the spot. The error bars include the uncertainty in the planet-center determination and the spot location measurement. The spot size in a typical projection is ~ 6 pixels by 6 pixels. The true location of the spot is within 2 pixels of the brightness centroid at the 95% confidence level, so the 1σ error bar is < 1 pixel. The uncertainty in the planet-center determination is comparatively small. For an 80-point ring-edge fitting, the 1σ error is 0.1 pixel for x_0 and 0.3 for y_0 . One can therefore reasonably assume the error is 1 pixel for both x_p and y_p . This uncertainty translates to $\sim 2^\circ$ in longitude. With these uncertainties, the straight line with the best overall fit to the data has a slope of $-0.060^\circ \pm 0.008^\circ$ per day. For the brief period from 9 to 18 November, the slope is greater than, and with the opposite sense to, the overall slope (Fig. 3, inset). Most of the motion of the spot over the entire period from November 1990 to June 1991 is in longitude. A formal fit to the latitude data over this period shows a change of only $0.93^\circ \pm 0.48^\circ$.

These errors include only measurement uncertainties. They do not include the probability that there may be small, real variations from straight line motion. Although there are only two data points from June 1991, they were planned, with the experience of the November data, so the spot was perfectly positioned for one measurement at each wavelength. As expected, the two data points from June in Fig. 3 agree extremely well with each other. There is no information about possible short-term slope changes in June that would be analogous to the November data (Fig. 3, inset). So the small error assigned to the general slope of the HST data is only a formal result.

Fig. 3. Time variation of the longitude of the polar spot with respect to system III during the period from November 1990 to June 1991. (Inset) Blowup of the period 9 to 11 November. The slope during the November period was greater than, and of the opposite sense to, the slope for the longer period.



From polar projections of seven Voyager images taken over a period of ~ 270 days in 1980 and 1981, Godfrey (2) obtained a spot drift of $-0.040^\circ \pm 0.003^\circ$ per day with respect to system III. Our value represents an $\sim 50\%$ increase in the magnitude of the drift rate compared with Godfrey's. As Godfrey (2) first pointed out, this drift could merely be a result of the inaccuracy in the present standard rotation rate of system III. To improve further this standard rotation rate, we reanalyzed the Voyager dataset, adding several points to Godfrey's data, including post-encounter observations for both Voyager 1 and Voyager 2. Combining the Voyager and HST observations, we calculated the longitude drift of the spot with respect to system III over a period of ~ 11 years (Fig. 4). Of course, this assumes that the polar spot observed in the HST images is the same spot observed by the Voyager.

Within the Voyager data are examples

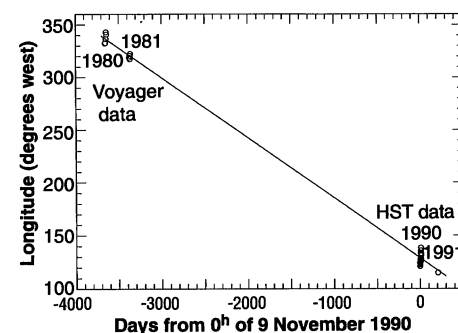


Fig. 4. Time variation of the longitude of the polar spot during the period from November 1980 to June 1991, based on both Voyager and HST data. The slope of the long-period drift is similar to the general slope in Fig. 3, which suggests that the much different slope during the brief interval shown in the inset to Fig. 3 is a transient effect superimposed on the general trend. The Voyager data also show evidence of short-term motions of magnitude similar to the HST data.

of short-term departures from the general trend, analogous to the inset in Fig. 3. With that understanding, the best fitting line has an overall drift of -0.0569° per day, in fair agreement with both the Voyager and HST drifts measured over hundreds of days. The fact that the HST drift is much closer to the longer term mean may be attributable to a fortuitous placement of the two coincident, accurate observations in June 1991 very near the mean position.

Because the value -0.0569° per day refers to a much longer time base line and is therefore less sensitive to temporary departures from the mean, we believe that it determines the best value for the rotation rate of system III so far. The rotation rate of Saturn's system III given by Desch and Kaiser (3) is $810.794^\circ \pm 0.148^\circ$ per day. The revised value, on the basis of this interpretation, is $810.737^\circ \pm 0.008^\circ$ per day.

There is also a short-term motion in the November 1990 images. The line in Fig. 3 that best fits the data from these images gives a rotation rate of $0.96^\circ \pm 0.10^\circ$ per day in the opposite direction to, and much faster than, the long-term drift. This rate implies a velocity of 3.27 ± 0.34 m/s. The time scale of this short-term motion is at least 9 days, and the deviation of the spot from its average value can be as large as 4.3° in longitude or ~ 1250 km. As noted above and by Godfrey (2), there were similar short-term motions in the Voyager data (Fig. 4). Systematic studies of short-term variation in the spot location will be an interesting task for future HST observations. In addition, the HST has the unique capability of verifying the continuous existence of this spot over long time frames.

Allison *et al.* (10) treated the hexagon as a planetary wave stimulated by the associated spot. In this study, we have shown that the spot and hexagon are both long-lived features of Saturn; since they were discovered, we have not seen one without the other. The long-term movement of the spot is also closely related to Saturn's internal rotation. Observations of this relation are consistent with the spot's being deeply rooted in Saturn's interior, acting as a stimulus in the polar jet and creating a wave structure visualized as the polar hexagon. We look forward to HST observations between 1996 and 2010 to see if the southern hemisphere has a structure and stability similar to that of the northern hexagon and spot.

REFERENCES AND NOTES

1. D. A. Godfrey, *Icarus* 76, 335 (1988).
2. ———, *Science* 247, 1206 (1990).
3. M. D. Desch and M. L. Kaiser, *Geophys. Res. Lett.* 8, 253 (1981).
4. J. A. Westphal *et al.*, *Icarus* 100, 485 (1992).
5. J. A. Westphal *et al.*, *Astrophys. J.* 369, L51 (1991).

6. T. R. Lauer, *Publ. Astron. Soc. Pac.* 101, 445 (1989).
7. C. C. Cunningham and D. M. Anthony, *Icarus*, in press.
8. L. B. Lucy, *Astron. J.* 79, 745 (1974).
9. The transformation from the coordinates in polar projection (x_p, y_p) to the corresponding coordinates in γ -projection (x', y') is given by

$$\begin{aligned} x' &= x_p \cos \gamma - \frac{b}{a} \sqrt{a^2 - r_p^2} \sin \gamma \\ y' &= y_p \end{aligned} \tag{1}$$

where $r_p = \sqrt{x_p^2 + y_p^2}$ is the distance of the point from the pole in polar projection and γ is the angle between the line of sight and the south-north axis of the planet. One obvious restriction on (x_p, y_p) for the transformation is $r_p \leq a$. Another restriction is

$$\frac{x_p}{\sqrt{a^2 - r_p^2}} \geq -\frac{a}{b \tan \gamma} \tag{2}$$

Otherwise, the point (x_p, y_p) is not visible in the

γ -projection. To determine the planetocentric latitude and longitude of the spot from the polar-projected image, we used

$$\tan \theta = \frac{a}{b} \frac{r_p}{\sqrt{a^2 - r_p^2}} \quad \cos \phi = \frac{x_p}{r_p} \tag{3}$$

where θ is measured from the north pole and ϕ is measured from the central meridian.

10. M. Allison, D. A. Godfrey, R. F. Beebe, *Science* 247, 1061 (1990).
11. We acknowledge the National Space Science Data Center (NSSDC) and the imaging-team leader from the Voyager project, B. A. Smith, for providing the Voyager images used in this analysis. C.D.B. thanks the National Academy of Sciences-National Research Council associateship program for providing the opportunity to process these data while at the NASA Goddard Space Flight Center.

15 September 1992; accepted 19 January 1993

Ground-Based Observations of Saturn's North Polar Spot and Hexagon

A. Sanchez-Lavega, J. Lecacheux, F. Colas, P. Laques

Ground-based observations of two conspicuous features near the north pole of Saturn, the polar vortex and the hexagonal wave structure, were made from July 1990 to October 1991, 10 years after their discovery. During this period the polar spot drifted in longitude, relative to system III, by -0.0353° per day on average. Superimposed on this mean motion, the spot also underwent short-term rapid excursions in longitude of up to $\sim 14^\circ$ at rates of up to $\sim 1^\circ$ per day. The spot also exhibited irregular variations in its latitude location. A combination of these data together with those obtained by Voyager 1 and 2 in 1980 and 1981 shows that the spot drifted -0.0577° per day for the 11-year interval from 1980 to 1991. The large lifetime of both features indicates that they are insensitive to the strong variations in the seasonal heating of the cloud layers in the upper polar atmosphere.

Voyager images of Saturn obtained in 1980 and 1981 revealed the presence of a hexagonal cloud structure located at planetographic latitude 78.7°N encircling the north pole (1). Associated with it, an oval spot, nicknamed Big Bertha by the Voyager imaging team (2), was observed impinging on the southern flank of one of the hexagon edges at 75.9°N . Both features were nearly stationary with respect to the planet's internal rotation (3). We present here ground-based observations of both features 10 years after their discovery and discuss the implications for their motions and structure. We used the 1.05-m-diameter telescope at Pic-du-Midi Observatory to make the measurements. The telescope was equipped with a charge-coupled device (CCD) camera and a

large set of filters covering the spectral range from 0.4 to 1 μm , including narrow-band interference filters centered in the methane absorption bands at 0.619, 0.725, and 0.899 μm (4). Although Saturn had a low declination and altitude above the horizon during the observing period, the usual excellent atmospheric conditions at Pic-du-Midi Observatory and the tilt of the planet as seen from the Earth (20° to 23°) allowed us to observe the polar features from July 1990 to December 1991. Data were available for 23 nights covering a period of 469 days.

Our first observation of the polar spot was made on 4 July 1990 (5). These images also revealed the hexagon, as shown in Fig. 1. The hexagon had been detected on a set of images obtained on 29 June 1989, although the polar spot was not visible because it was on the rear hemisphere. We performed measurements on the latitude and longitude location of the spot center and edges on different sets of frames obtained each night (6). The main source of error arises from the determination of the planet limbs and from the position of the spot itself. We estimate that the average errors are $\sim 2^\circ$ in latitude

A. Sanchez-Lavega, Departamento Fisica Aplicada I, Escuela Técnica Superior de Ingenieros Industriales y de Telecomunicación, Universidad del País Vasco, Alda. Urquijo s/n, 48013 Bilbao, Spain.
 J. Lecacheux, Département de Recherches Spatiales, Observatoire Paris-Meudon, 92190 Meudon, France.
 F. Colas, Bureau des Longitudes, 77 Avenue Denfert Rochereau, 75014 Paris, France.
 P. Laques, Observatoire Pic-du-Midi, 65200 Bagneres-de-Bigorre, France.